Supporting Information

Variance Spectroscopy

Jason K. Streit, Sergei M. Bachilo, Stephen R. Sanchez, Ching-Wei Lin, and

R. Bruce Weisman

1. Data Analysis

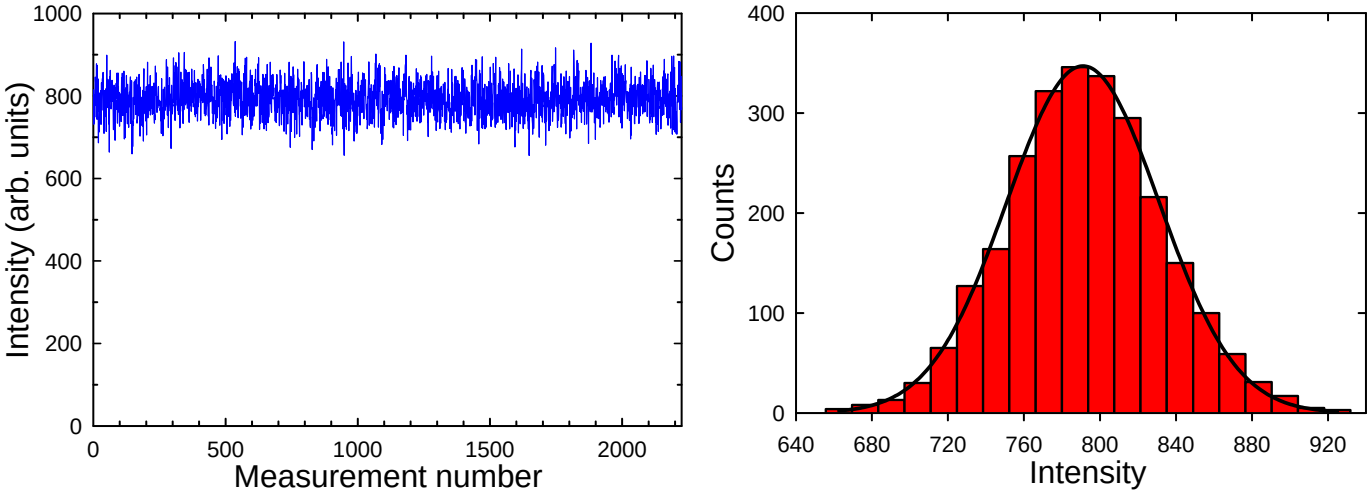

Figure S1. (Left) Typical single-wavelength emission intensities for a full variance dataset. (Right) Histogram of those single-wavelength signal intensities with a Gaussian best-fit shown as the solid curve.

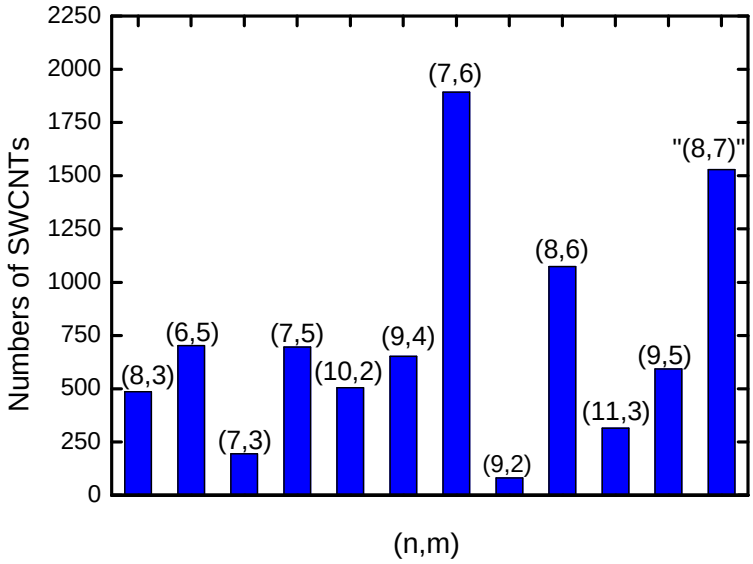

Figure S2. Deduced particle number abundances from the sample analysis of Fig. 2 in the main text. Each bar is labeled with the main (*n*,*m*) species it represents, but some contain contributions from other spectrally overlapping species, especially the one labeled "(8,7)".

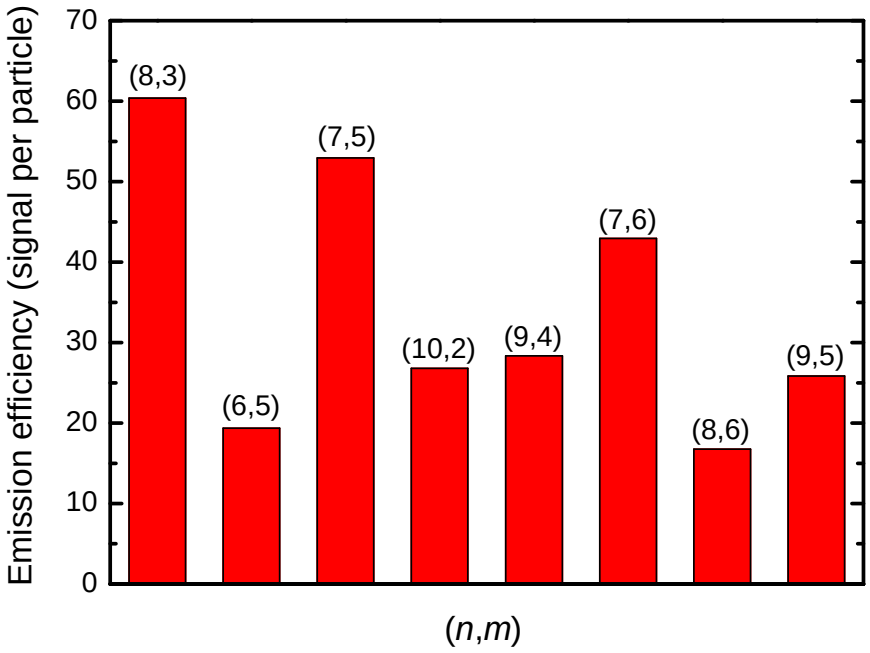

Figure S3. Emission efficiency per particle for various (*n*,*m*) species, as deduced from the variance analysis shown in Fig. 2 of the main text. These values are not corrected for differing (*n*,*m*)-specific absorption cross sections at the 660 nm excitation wavelength.

2. Covariance Profiles

As explained in the main text, the formula for covariance at two wavelengths is

$$\mathrm{cov}\left(\lambda_j,\lambda_k\right)=\frac{1}{M}\sum_{i=1}^{M}\left(I_i\left(\lambda_j\right)-\bar{I}\left(\lambda_j\right)\right)\left(I_i\left(\lambda_k\right)-\bar{I}\left(\lambda_k\right)\right)$$

For SWCNT samples, each factor inside the sum is a superposition of emission contributions at one wavelength from a discrete set of nanotube species, (*n*,*m*):

$$I_i\left(\lambda_k\right)-\bar{I}\left(\lambda_k\right)=\sum_{(n,m)}\left[I_i\left(\lambda_k\right)_{(n,m)}-\bar{I}\left(\lambda_k\right)_{(n,m)}\right]$$

This can be rewritten in terms of intensities at $\left(\lambda_{\max}\right)_{(n,m)}$, the peak emission wavelength of species (*n*,*m*), which is proportional to intensity at arbitrary wavelength $\left(\lambda_k\right)_{(n,m)}$:

$$\sum_{(n,m)}\left[I_i\left(\lambda_k\right)_{(n,m)}-\bar{I}\left(\lambda_k\right)_{(n,m)}\right]=\sum_{(n,m)}\left[I_i\left(\lambda_{\max}\right)_{(n,m)}-\bar{I}\left(\lambda_{\max}\right)_{(n,m)}\right]\frac{\bar{I}\left(\lambda_k\right)_{(n,m)}}{\bar{I}\left(\lambda_{\max}\right)_{(n,m)}}$$

The covariance expression then becomes:

$$\mathrm{cov}\left(\lambda_j,\lambda_k\right)=\frac{1}{M}\sum_{i=1}^{M}\left\{\left(\sum_{(n,m)}\left[I_i\left(\lambda_{\max}\right)_{(n,m)}-\bar{I}\left(\lambda_{\max}\right)_{(n,m)}\right]\frac{\bar{I}\left(\lambda_j\right)_{(n,m)}}{\bar{I}\left(\lambda_{\max}\right)_{(n,m)}}\right)\left(\sum_{(n,m)'}\left[I_i\left(\lambda_{\max}\right)_{(n,m)'}-\bar{I}\left(\lambda_{\max}\right)_{(n,m)'}\right]\frac{\bar{I}\left(\lambda_k\right)_{(n,m)'}}{\bar{I}\left(\lambda_{\max}\right)_{(n,m)'}}\right)\right\}$$

or

$$\mathrm{cov}\left(\lambda_j,\lambda_k\right)=\frac{1}{M}\sum_{i=1}^{M}\left\{\sum_{(n,m)}\sum_{(n,m)'}\left[I_i\left(\lambda_{\max}\right)_{(n,m)}-\bar{I}\left(\lambda_{\max}\right)_{(n,m)}\right]\left[I_i\left(\lambda_{\max}\right)_{(n,m)'}-\bar{I}\left(\lambda_{\max}\right)_{(n,m)'}\right]\left(\frac{\bar{I}\left(\lambda_j\right)_{(n,m)}}{\bar{I}\left(\lambda_{\max}\right)_{(n,m)}}\right)\left(\frac{\bar{I}\left(\lambda_k\right)_{(n,m)'}}{\bar{I}\left(\lambda_{\max}\right)_{(n,m)'}}\right)\right\}$$

For a sample of individualized, independent particles, the double sum over species reduces to a single sum with $(n,m)'=(n,m)$:

$$\mathrm{cov}\left(\lambda_j,\lambda_k\right)=\frac{1}{M}\sum_{i=1}^{M}\left\{\sum_{(n,m)}\left[I_i\left(\lambda_{\max}\right)_{(n,m)}-\bar{I}\left(\lambda_{\max}\right)_{(n,m)}\right]^2\left(\frac{\bar{I}\left(\lambda_j\right)_{(n,m)}\bar{I}\left(\lambda_k\right)_{(n,m)}}{\bar{I}^{\,2}\left(\lambda_{\max}\right)_{(n,m)}}\right)\right\}$$

Changing the order of summation gives:

$$\mathrm{cov}\left(\lambda_j,\lambda_k\right)=\sum_{(n,m)}\left\{\left(\frac{\bar{I}\left(\lambda_j\right)_{(n,m)}\bar{I}\left(\lambda_k\right)_{(n,m)}}{\bar{I}^{\,2}\left(\lambda_{\max}\right)_{(n,m)}}\right)\sum_{i=1}^{M}\frac{\left[I_i\left(\lambda_{\max}\right)_{(n,m)}-\bar{I}\left(\lambda_{\max}\right)_{(n,m)}\right]^2}{M}\right\}$$

The second sum is the intensity variance of the species (*n*,*m*) at its emission peak, so it is equal to the square of mean fluorescence intensity at its peak divided by $\mathrm{n}_{(n,m)}$, the average observed number of particles of that species:

$$\mathrm{cov}\left(\lambda_j,\lambda_k\right)=\sum_{(n,m)}\left\{\left(\frac{\bar{I}\left(\lambda_j\right)_{(n,m)}\bar{I}\left(\lambda_k\right)_{(n,m)}}{\bar{I}^{\,2}\left(\lambda_{\max}\right)_{(n,m)}}\right)\left[\sigma^2\left(\lambda_{\max}\right)_{(n,m)}\right]\right\}=\sum_{(n,m)}\left\{\left(\frac{\bar{I}\left(\lambda_j\right)_{(n,m)}\bar{I}\left(\lambda_k\right)_{(n,m)}}{\bar{I}^{\,2}\left(\lambda_{\max}\right)_{(n,m)}}\right)\left[\frac{\bar{I}^{\,2}\left(\lambda_{\max}\right)_{(n,m)}}{\mathrm{n}_{(n,m)}}\right]\right\}$$

This reduces to the simple expression:

$$\mathrm{cov}\left(\lambda_j,\lambda_k\right)=\sum_{(n,m)}\frac{\bar{I}\left(\lambda_j\right)_{(n,m)}\bar{I}\left(\lambda_k\right)_{(n,m)}}{\mathrm{n}_{(n,m)}}$$

This result shows how to interpret the spectral profile obtained from the covariance matrix by fixing one coordinate at wavelength λ_k and plotting covariance values as a function of the other wavelength coordinate, λ_j (for example Figure 3b, red curve). The resulting profile, for a sample containing

independent particles, will be a linear superposition of mean fluorescence spectra from all (*n*,*m*) species in the sample, each weighted by the ratio of its fluorescence intensity at λ_k to the number of (*n*,*m*) particles (its emissive efficiency at λ_k under the experimental excitation conditions). If λ_k is chosen near the emission peak of one species, then the profile can be strongly dominated by the spectrum of that single species. In addition, particles in the sample that emit weakly (such as damaged nanotubes or impurities) will contribute very little to the covariance spectral profile, even if they are present at high abundances and collectively give a significant amount of emission.

3. Details of flowing sample method

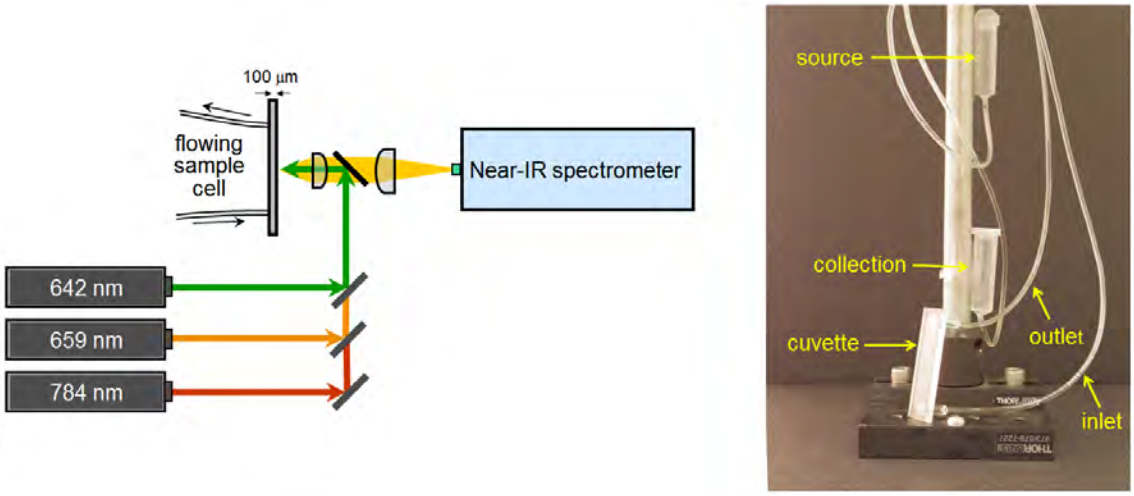

Figure S4. (left) Optical diagram of the flowing sample instrumental setup. (right) Image of the custom-built flow system, with the cuvette removed from the optical system for clarity.

Flow rate optimization

The magnitudes of the intensity fluctuations should be dependent on the flow rate of the sample, so it is important to choose a flow rate to maximize all fluctuations from sample compositions and reduce contributions from detector noise. To determine this optimum, variance spectroscopy measurements were performed on a SWCNT sample at sequentially increasing flow rates. As shown in Figure S5a, intensity variance is lowest when the smallest flow rates are used. This suggests that the measurements are not statistically independent of each other, presumably because multiple fluorescence spectra are being acquired from overlapping sample volumes. Figure S5b shows that when the flow rate is too large, the fluorescence fluctuations again decrease, an effect we attribute to flow averaging of the probed volume's composition during each 150 ms exposure time. Figure S5c-d plots the mean and variance of

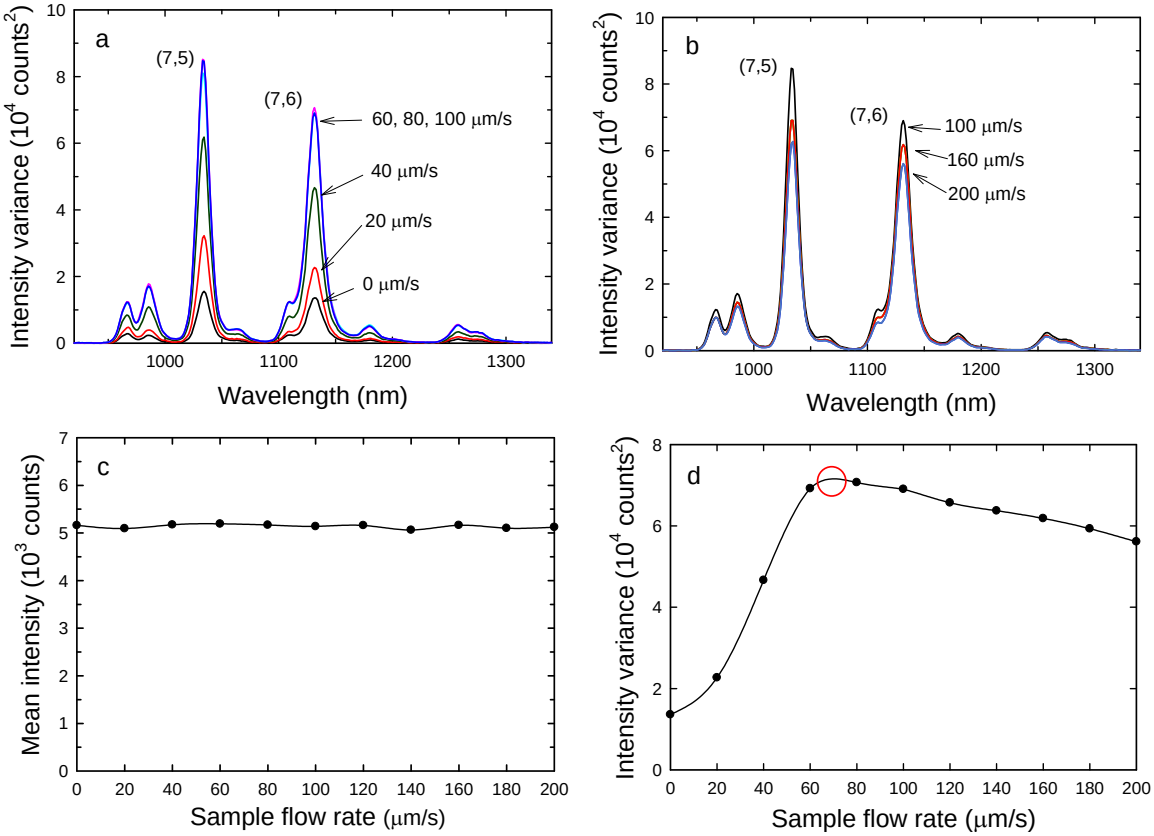

Figure S5. Finding the optimal flow rate. Measured variance spectra using flow rates ranging from 0 to 100 μm/s **(a)** and 100 to 200 μm/s **(b).** Mean **(c)** and variance **(d)** of the (7,6) emission peak plotted as a function of flow rate.

the (7,6) emission peak as a function of sample flow rate. Although the mean is unaffected by sample flow, the variance reaches an apparent maximum at an optimal linear flow rate of ~70 μm/s. Slight deviations from this value (~60 to 80 μm/s) do not significantly change the variance, which means that small differences in flow rate should not compromise the deduced concentration values. We estimate the effective diameter of our probed volume in the sample to be ~25 μm by multiplying the optimum flow rate by the acquisition interval (the sum of the exposure and dead times).

This optimal flow rate will also depend on the specific exposure time used in the analysis. Larger fluctuations can theoretically be achieved by using more dilute samples combined with longer exposure times and slower flow rates. However, the overall processing time then becomes significantly larger, making this method less convenient and practical. A flow rate of approximately 70 μm/s was used for all measurements in this study.

4. Laser Stability Tests

We tested the stability of the excitation lasers used in the flowing sample method in order to ensure that measured fluorescence intensity fluctuations were not dominated by changes in excitation power. For this, we measured the relative fluctuations (standard deviation / mean) with the flowing sample apparatus on a highly concentrated SWCNT sample, in which intensity variations arising from nanotube concentration are expected to be minimal. The relative fluctuations, plotted in Figure S6 for all three excitation wavelengths, were found to be less than 0.1%, or more than an order magnitude below the 1% to 8% fluorescence fluctuations measured for typical dilute SWCNT samples. We therefore conclude that effects relating to excitation laser instability are negligible when SWCNT intensity fluctuations are relatively large (greater than 1%) and can be ignored for the present study.

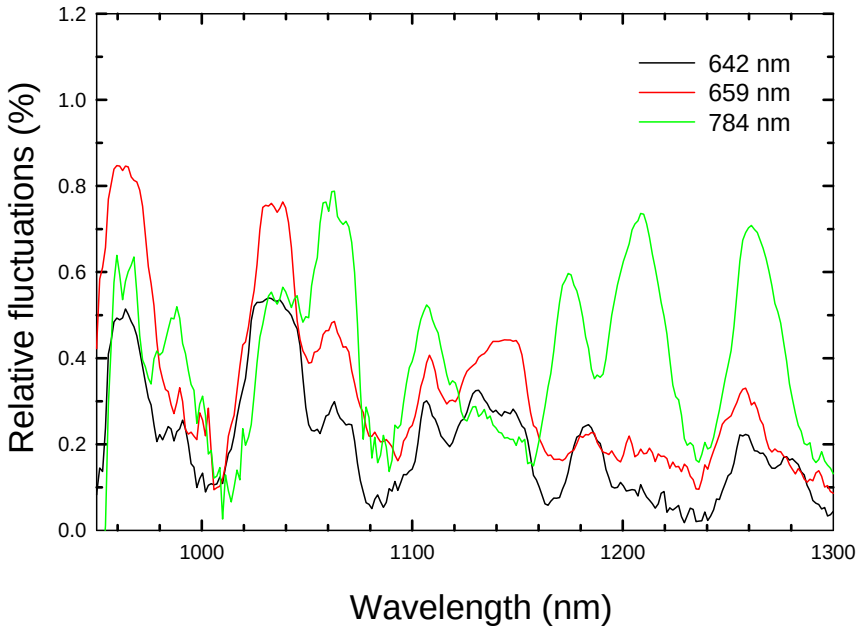

Figure S6. Estimated laser noise levels from three excitation lasers as found by measuring the relative fluorescence fluctuations of a highly concentrated SWCNT sample.

For a similar stability test of the 660 nm diode laser used for excitation in the step scan measurements, we used a long-pass glass filter (Schott RG670) as a reference sample. Although this filter is not intended to be used as an emission source, it emits broad SWIR luminescence from a dense, static array of nanoparticles when excited with visible light. Emission spectra were captured with a 30 ms integration time and 450 ms dead time between measurements. The relative fluctuations

(standard deviation / mean) in the measured emission were found to be on the order of 0.05%. This value is two orders of magnitude below the fluctuations of typical SWCNT samples used in our study. This excitation laser therefore makes a negligible contribution to the reported variance spectra.

5. Dilution Tests

We checked the validity of concentration values deduced from variance spectra by performing a simple dilution test on a sample of SWCNTs dispersed in aqueous 1% sodium deoxycholate solution. Measurements were made on the original sample, on the sample after dilution by a volumetric factor of 1.4, and also after dilution by a factor of 2.0. Relative concentrations were determined by variance analysis for multiple spectral features following each dilution. Figure S7 shows dilution factors deduced from variance-derived abundances and from mean fluorescence intensities. The close agreement among these values indicates that variance spectroscopy can be used to accurately determine relative changes in species concentrations.

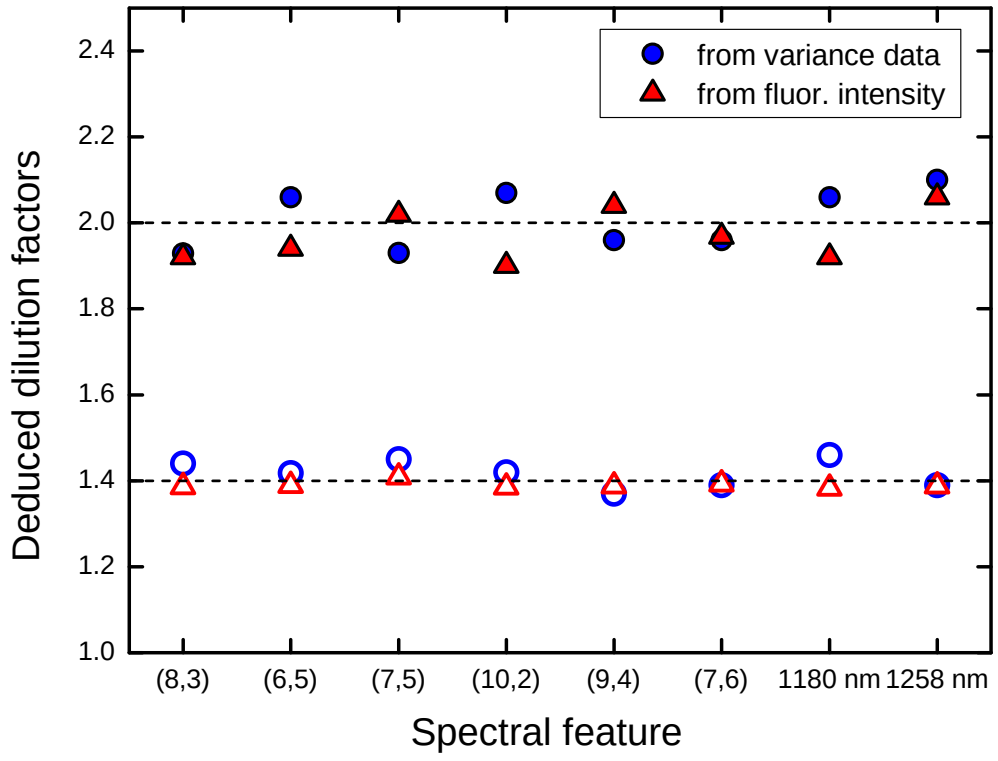

Figure S7. Relative nanotube concentrations measured after twice diluting a SWCNT sample by a factor of 1.4. The graph shows dilution factors for several (n,m) peaks deduced from variance analysis (blue circles), emission intensities (red triangles) and known volumetric ratios (dashed lines).

6. Aggregation Effects on Covariance Spectra

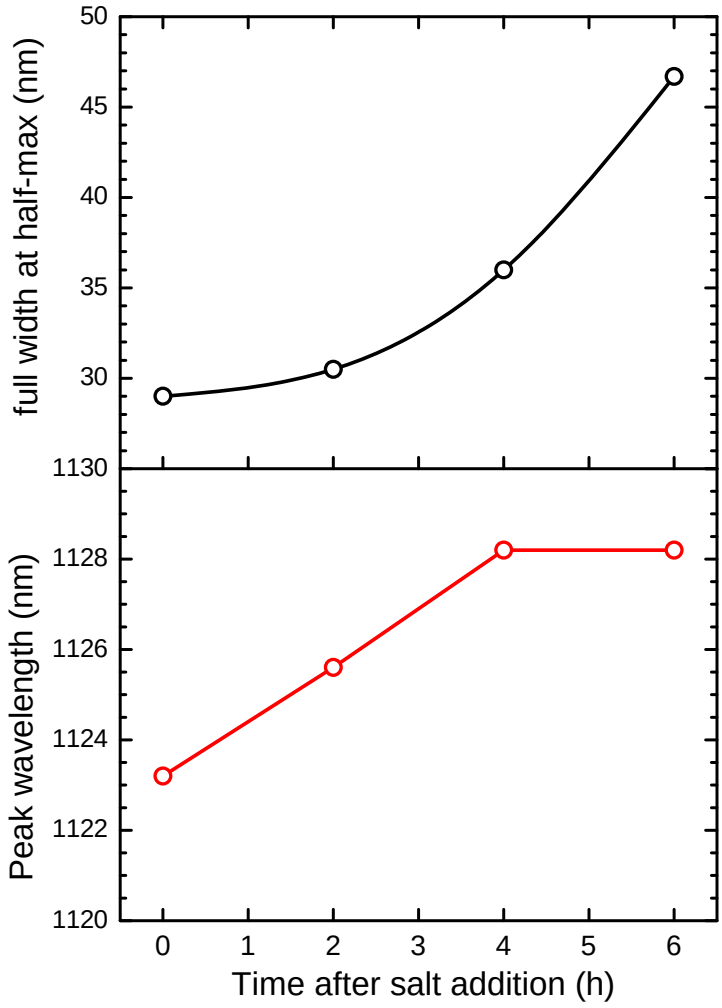

Figure S8. Full-widths at half-maximum and peak wavelengths of the main peak in the (7,6) covariance spectra of Fig. 4c, plotted against aggregation time after salt addition.

Figure S8 quantifies the changes in peak position and width observed for the (7,6) covariance spectra of Fig. 4c as the sample formed loose aggregates. The dominant contribution to peak broadening is likely the growth in nearby covariance peaks assigned to loose aggregates. However, at least part of the observed red-shift and broadening may reflect a change in (7,6) dielectric environments from proximity to other SWCNTs.

7. Unabridged citation for Reference 5 of the main text

(5) O'Connell, M. J.; Bachilo, S. M.; Huffman, C. B.; Moore, V.; Strano, M. S.; Haroz, E.; Rialon, K.; Boul, P. J.; Noon, W. H.; Kittrell, C., Ma, J.; Hauge, R. H.; Weisman, R. B.; Smalley, R. E. Band-Gap Fluorescence From Individual Single-Walled Carbon Nanotubes. *Science* **2002,** *297*, 593-596.